Original Article

An investigation into the oil transport and starvation of piston ring pack

SR Bewsher[1], M Mohammadpour[1] , H Rahnejat[1], G Offner[2]
and O Knaus[2]

Abstract

In order to accurately predict the lubricant film thickness and generated friction in any tribological contact, it is important to determine appropriate boundary conditions, taking into account the oil availability and extent of starvation. This paper presents a two-dimensional hydrodynamic model of a piston ring pack for prediction of lubricant film thickness, friction and total power loss. The model takes into account starvation caused by reverse flow at the conjunctional inlet wedge, and applied to a ring pack, comprising a compression and scraper ring. Inlet boundaries are calculated for an engine cycle of a four-cylinder, four-stroke gasoline engine operating at 1500 r/min with conditions pertaining to the New European Drive Cycle. The analysis shows the two main sources of starvation: first, due to a physical lack of inlet meniscus and second, due to reverse flow at the inlet wedge significantly affecting the prevailing conditions from the generally assumed idealised boundary conditions. Such an approach has not hitherto been reported in literature.

Keywords

Piston ring pack, inlet starvation, zero reverse flow inlet boundary, mixed hydrodynamics, friction

Introduction

Concern for pollution levels and greenhouse gas emissions has resulted in increasingly stringent directives and legislation affecting the automotive sector. Therefore, power train efficiency is now the key objective to alleviate these concerns.[1] Frictional power losses account for nearly 20% of all the losses in passenger vehicle internal combustion engines, with the piston–cylinder system share of these being 40–45%.[2–4] To be able to mitigate these losses, it is essential to have detailed predictive methods. With engine downsizing a greater emphasis is put upon increased power-to-weight ratio in order to maintain or improve upon engine performance. With increased in-cylinder pressures, particularly during the power stroke, the conjunctional gaps between the piston ring pack and cylinder liner diminish. This can result in higher instances of direct interaction of contacting surfaces, thus increased friction and wear.[5,6] It is therefore essential to be able to predict the lubricant film thickness for any given set of design and operational parameters.

There have been many contributions in the study of piston rings-to-cylinder liner contacts, featuring the effects of conjunctional geometry, surface topography, lubricant rheology, operating conditions (gas pressure, load, speed and temperature) and even surface materials, coatings and any surface modification.[7–22] The ultimate aim is to reduce friction and wear.

In most applications, the piston ring pack comprises two compression rings, an oil control ring and a scraper ring. A model is required to determine the oil transport between these rings, in particular the quantity of oil left on the liner surface in the wake of a leading ring. This constitutes the inlet meniscus for a trailing ring which crucially affects its prevailing regime of lubrication. This issue is particularly important during the power stroke, where there is reduced lubricant availability at the top ring, with its inlet boundary starved of lubricant at high in-cylinder pressures. One of the most widely used oil transport models is that of Tian et al.[14] It makes use of the average flow model of Patir and Cheng.[23,24]

[1]Wolfson School of Mechanical, Electrical and Manufacturing Engineering, Loughborough University, Loughborough, UK
[2]AVL List GmbH, Graz, Austria

Corresponding author:
SR Bewsher, Loughborough University, Wolfson Building, Loughborough, Leicestershire LE11 3TU, UK.
Email: s.r.bewsher@lboro.ac.uk

A one-dimensional model was developed to predict the lubricant film thickness and generated friction. The model was then extended to the case of three rings, assuming that in the downstroke sense of the piston there would always be a sufficient volume of lubricant available for the oil control ring conjunction. The boundary conditions imposed for the inlet considered a wetting location at the leading edge of the ring. The usual Reynolds exit boundary condition was replaced by a non-separation film condition, where the squeeze film lubrication may be considered to be dominant. It was shown that the top compression ring is able to carry a quantity of lubricant to the region above the top dead centre (TDC) of the oil control ring during the compression stroke. This is due to raised pressure in the region below the top ring. Surface roughness was also found to contribute significantly to the mechanism of oil transport.

Using floating liners to directly measure frictional characteristics of piston–cylinder system, it was found that boundary and mixed regimes of lubrication are prevalent at TDC reversals.[25–27] The same experimental results indicated that at the inlet there would be an insufficient supply of lubricant for the compression ring during the upstroke motion of the piston. Therefore, inlet starvation should be taken into account when predicting the frictional losses. There are two main sources of starvation. One is due to a physical lack of lubricant which requires modelling of oil transport, comprising the inclusion of the entire ring pack to estimate the quantity of available lubricant for any trailing ring. The other is starvation due to reverse (counter) flow at the inlet boundary.[28,29] This requires a numerical or an analytical flow analysis to predict the inlet stagnation boundary, beyond which no reverse flow occurs and the build-up of contact pressure commences. Post stagnation point, it can be assumed that the remaining volume of lubricant contributes to the oil flow into the conjunction proper. Tipei[30,31] provided an analytical method for this purpose, predicting the location of the inlet stagnation boundary. Using this approach, it is possible to determine where an inlet boundary condition should be placed in a numerical model, as opposed to assuming an idealised fully flooded inlet at the edge of the ring, which is often assumed. This assumption can lead to over-optimistic predictions of lubricant film thickness. The results with realistic boundary conditions would be closer in conformance with the experimental measurements.[32]

This paper presents a method for predicting inlet lubricant availability for piston ring pack, including the effect of starvation. The model comprises the leading and trailing compression rings' conjunctions, as well as the oil transport between them. Tipei's potential flow model approach is used in order to predict the zero reverse inlet boundary and estimate the extent of starvation. This approach has not hitherto been reported in literature.

Numerical method

Reynolds equation in its two-dimensional form for a compressible piezo-viscous lubricant can be expressed as

$$
\frac{\partial}{\partial x}\left(\frac{\rho h^3}{6\eta}\frac{\partial p}{\partial x}\right) + \frac{\partial}{\partial y}\left(\frac{\rho h^3}{6\eta}\frac{\partial p}{\partial y}\right)
$$
$$
= \frac{\partial(\rho U h)}{\partial x} + \frac{\partial(\rho V h)}{\partial y} + 2\frac{\partial(\rho h)}{\partial t} \tag{1}
$$

The above form of the equation includes flow in the direction of entraining motion, x, as well as side leakage, y. In the current analysis the side-leakage Couette flow is neglected as $V = 0$.

It is important to take into account the effect of pressure on the density of lubricant, especially in assemblies such as the piston ring pack. The Dowson and Higginson density model[33] is used

$$
\rho = \rho_0\left(1 + \frac{0.6\times10^{-9}(p-p_0)}{1+1.7\times10^{-9}(p-p_0)}\right)
$$
$$
\times\left[1 - 0.65\times10^{-3}(\theta-\theta_0)\right] \tag{2}
$$

where ρ_0 is the lubricant density at ambient pressure and reference temperature θ_0 and p is the absolute pressure.[34] The viscosity of the lubricant is also pressure dependent. Barus law is commonly used in order to find its temperature and pressure dependency.[35] However, a more accurate model for lubricant viscosity is provided by Roelands,[36] which was further developed by Houpert[37]

$$
\eta = \eta_0(\alpha^* p) \tag{3}
$$

$$
\alpha^* p = [\ln(\eta_0 + 9.67)]
$$
$$
\times\left\{\left(\frac{\theta-138}{\theta_0-138}\right)^{-S_0}\left[\left(1+\frac{p}{p_0}\right)^Z - 1\right]\right\} \tag{4}
$$

The constants Z and S_0 are independent of both pressure and temperature

$$
Z = \frac{\alpha}{5.1\ \times\ 10^9[\ln(\eta_0)+9.67]} \tag{5}
$$

$$
S_0 = \frac{\beta(\theta_0-138)}{\ln(\eta_0)+9.67} \tag{6}
$$

The minimum lubricant film thickness h_m is obtained as[34]

$$
h(x,y,t) = h_m(t) + h_s(x) \tag{7}
$$

This equation does not take into account any localised deflection of the contiguous bodies in contact or their thermoelastic deformation. Bolander et al.[38] and

Mishra et al.[39] show that the generated contact pressures in ring–liner conjunction are insufficient to cause any localised contact deflection. In practice, the rings can undergo modal behaviour as shown by Baker et al.[40] Since this analysis is based on a passenger vehicle, the effects of elastic deformation are not taken into account in the current analysis.[41]

The ring profile is assumed to be parabolic

$$h_s(x) = \frac{c(x - b/2)^2}{\left(b/2\right)^2} \qquad (8)$$

This approach can be adopted and any profile for either the top compression or scraper ring can be incorporated in the model. Extra rings such as the oil control ring can also be added. Since this study focuses on tackling the numerical solution for starvation and reverse flow, for proof of concept it is more suitable to use two identical rings.

The radial outward forces acting on the top compression ring, pressing it into the cylinder liner are

$$F = F_e + F_g \qquad (9)$$

The gas force, F_g, acts behind the inner rim of the ring, where the combustion pressure, p_g, is obtained from the combustion pressure curve in Figure 4

$$F_g = p_g bl \qquad (10)$$

Assuming the ring has a rectangular cross section, the elastic ring tension force, F_e, is found as a function of the elastic pressure, p_e as

$$F_e = p_e bl \qquad (11)$$

$$p_e = \frac{gEI}{3\pi b r_0^4} \qquad (12)$$

$$I = \frac{1}{12} bd^3 \qquad (13)$$

In the current analysis, as in the majority of the reported studies, an ideal right circular cylindrical liner is assumed, thus the compression and scraper rings conform to the bore. In practice, the cylinder is out of round as described by Ma et al.[19] and Rahmani et al.[16]

It is assumed that the hydrodynamic reaction and asperity contact forces act on the ring running face and equilibrate the applied ring tension and gas forces. The hydrodynamic reaction is obtained as

$$W_h = \iint p \, \mathrm{d}x \mathrm{d}y \qquad (14)$$

The Greenwood and Tripp[42,43] method is used to calculate the asperity contact load within the conjunction

$$W_a = \frac{16\sqrt{2}}{15} \pi (\zeta K \sigma)^2 \sqrt{\frac{\sigma}{K}} E' A F_{5/2}(\lambda) \qquad (15)$$

The roughness parameter $(\zeta K \sigma)$ is found using surface topographical measurements and σ/K is a measure of a typical asperity slope.[34] $\lambda = \frac{h}{\sigma}$ is the Stribeck oil film parameter. $\lambda = 3$ is the critical value below which some asperity interactions occur.

The total generated friction is

$$f = f_b + f_v \qquad (16)$$

The boundary friction due to interaction of asperities is calculated as

$$f_b = \tau_0 A_a + \varsigma W_a \qquad (17)$$

where the shear strength of asperities (ς) is found using an atomic force microscope in lateral force mode. The total area of the tips of the asperities A_a is determined as[41,42]

$$A_a = \pi^2 (\zeta K \sigma)^2 A F_{3/2}(\lambda) \qquad (18)$$

The viscous friction is obtained as

$$f_v = \int_0^l \int_0^b \tau \, \mathrm{d}x \, \mathrm{d}y \qquad (19)$$

where, shear stress, τ, is calculated as

$$\tau = \left| -\frac{dp}{dx} \vec{\nabla} p \frac{h}{2} + \frac{\eta U}{h} \frac{\vec{V}}{} \right| \qquad (20)$$

Boundary conditions, starvation due to the reverse flow

Fully flooded condition is assumed in the majority of reported hydrodynamic analyses and has been used in the case of piston ring–cylinder liner conjunction.[15,16,20,44] This assumes that a sufficient volume of lubricant would be available at the inlet of each ring in the ring pack. Hence, the edge of the ring is taken as the position of the inlet meniscus. Thus

$$p_{x=-b/2} = P_a \qquad (21)$$

where P_a is the ring inlet pressure, which is assumed to be the crank-case (inter-ring) pressure in the piston downstroke motion, and the combustion chamber pressure in its upstroke sense. However, the in situ measured frictional characteristics, using floating
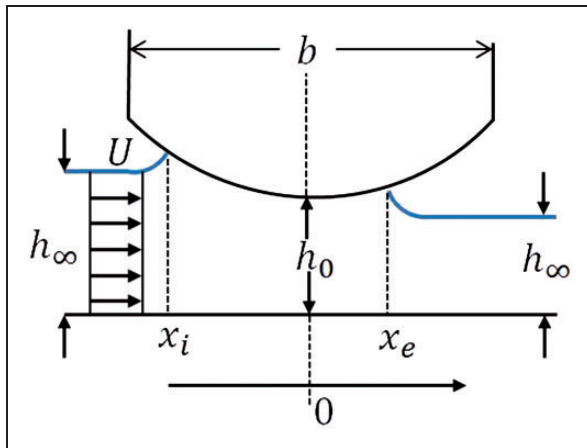
Figure 1. Definition of variables.

Figure 2. Velocity and rates of flow distribution with counter flow.[30]

Figure 3. Flow in the inlet region.[30]

liners show that boundary or mixed regimes of lubrication are prevalent for parts of the piston cycle.[22,25–27] This is partly because of an insufficient volume of lubricant at the conjunctional inlets, particularly for the top compression ring in the upstroke motion of the piston. This is a source of starvation. Furthermore, for partially flooded inlets, any excess supply of lubricant is subject to swirl and counter flows as shown in a detailed study by Shahmohamadi et al.[45]

Tipei[30] found that although the two-dimensional solution of Reynolds equation is applicable for practical problems, the justification of two-dimensional flow continuity condition is only valid for special cases. It was shown that only a fraction of the inlet-bound flow is actually drawn into the contact of the contiguous surfaces for any given geometry, load and speed, whilst forming swirl flows upstream of a stagnation point. The excess flow undergoes side leakage from the contact.[31]

Reverse flow at the inlet and consequent starvation

Figure 2 shows the total flow into the inlet wedge. Only a portion of this flow is entrained into the contact (Q_2), whilst some of the flow reverses outwards (i.e. reverse flow, Q_1, Q_3), depending upon the surface velocities of the contacting surfaces U_1 and U_2.

Figure 3 represents the inward flow motion, assuming upstream lubricant wetting of both the contacting surfaces. It can be seen that the flow field contains two inward bound vortices, generating a close streamline.

Tipei[30] provided a detailed explanation of the fluid film flow, depending upon the upstream flow dynamics as shown in Figure 3. The supplied fluid flow, q_1 and q_2, adhere to the surfaces, partially penetrating the load-carrying zone. The centre of the vortices, O_1 and O_2, lie on the contact normal A–A, which according to the theory of lubrication is the upstream limit for which the fluid film in Navier–Stokes equations can be simplified. Thus, one cannot assume that
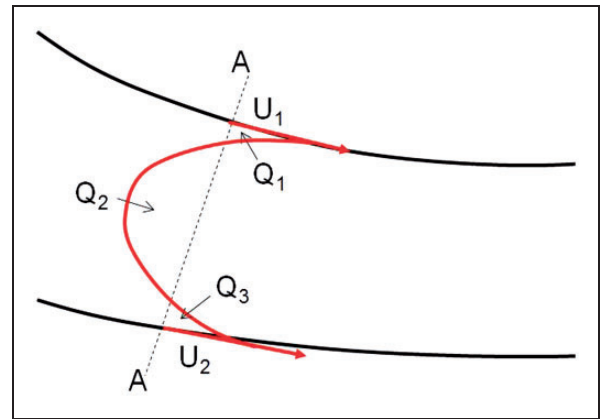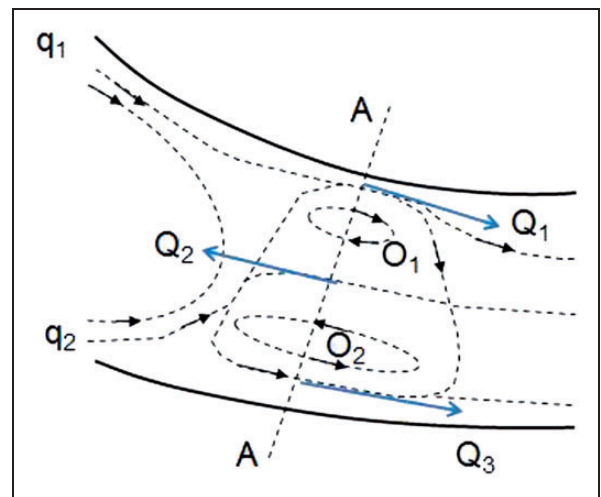
downstream of A–A the fluid would fill the gap entirely, or indeed neglect the velocity components normal to the surfaces. Using the method expounded by Tipei, it is possible to determine where an inlet boundary condition should be placed, as opposed to assuming an idealised fully flooded inlet.

Experimental studies on the effects of surface texturing in order to tackle starvation have shown that starvation occurs after each reversal, even when the contact is subject to fully flooded conditions. The change of direction makes the cavitated region of the outlet the new inlet region in the subsequent stroke.[46,47] It was also observed that the region of starvation can occur for 5% of the stroke. However, this will be dependent upon the viscosity of the lubricant.

Outlet boundary conditions are also affected when modelling piston rings due to the effect of cavitation. The Reynolds (or Swift–Steiber[48,49]) outlet boundary conditions can be applied, which determine the location of the lubricant film rupture along the entraining x-direction of the contact. Assuming that cavitation occurs in the direction of fluid flow, where the pressure

gradient diminishes, the cavitation pressure is taken to be half that of the cavity, although in most cases this is assumed to be at atmospheric pressure. It is also assumed that the lubricant flows between the air cavities, although the effect at the cavity–fluid interface is ignored. Arcoumanis et al.[50] conducted an experiment, which showed that predictions using the Swift–Steiber boundary conditions matched the experimental observations for the most of the engine stroke. Accordingly, the exit boundary conditions become

$$
\begin{cases}
p_{x=x_c} = P_{cav} \\
\left.\frac{\partial p}{\partial x}\right|_{x=x_c} = 0
\end{cases}
\tag{22}
$$

In the current analysis the cavitation pressure, P_{cav}, is considered to be the atmospheric pressure at the lubricant film rupture boundary: $x = x_c$.

Prediction of the location of boundary condition at the inlet

The primary focus of the current analysis is the effect of boundary conditions on the generated frictional losses due to starvation. Tipei[30] showed that the justification for two-dimensional Reynolds equation under the continuity of flow condition is only valid for special cases, although it is applicable for practical problems. It was shown experimentally that not all of the lubricant is drawn between the two contiguous surfaces for a given conjunctional geometry (wedge shape), load and speed. In fact, only a fraction of the in-bound lubricant is drawn into the contact.[51,52]

An analytical expression was obtained by Tipei[30] through application of Swift–Steiber boundary condition at the inlet and outlet of the contact ($dp/dx = 0$ and $P_{cav} = 0$). This is in order to maintain the continuity of flow condition between the film thickness at the inlet and the outlet exit boundaries

$$
\frac{\cosh \theta_e}{\cosh \theta_i} = 1 - \frac{f(k)}{6(1+k)}
\tag{23}
$$

and

$$
\tanh \theta_e - \left[1 - \frac{f(k)}{6(1+k)}\right] \tanh \theta_i
$$
$$
- \left[1 - \frac{f(k)}{6(1+k)}\right] \cosh \theta_i
\tag{24}
$$
$$
\times [arc\sin(\tanh \theta_e) - arc\sin(\tanh \theta_i)] = 0
$$

θ_e is the ratio of the lubricant film thickness at the exit to that at the centre of the contact, whilst θ_i is the same for the inlet position. k is the ratio of the velocities of the contiguous surfaces and $f(k)$ is a characteristic determined by the value of k through application of compatibility equation

$$
\cot^2 \pi \left[\frac{1}{2} - \frac{1-k}{f(k)}\right] - \cot^2 \pi \sqrt{\left[\frac{1}{2} - \frac{1-k}{f(k)}\right]^2 - \frac{2k}{f(k)}}
$$
$$
= \cot \pi \left(\frac{1}{2} - \frac{1-k}{f(k)} - \sqrt{\left[\frac{1}{2} - \frac{1-k}{f(k)}\right]^2 - \frac{2k}{f(k)}}\right)
$$
$$
\times \cot \pi \left(\frac{1}{2} - \frac{1-k}{f(k)} - \sqrt{\left[\frac{1}{2} - \frac{1-k}{f(k)}\right]^2 - \frac{2k}{f(k)}}\right)
\tag{25}
$$

where

$$
k = \frac{U_1}{U_2}
\tag{26}
$$

where U_1 and U_2 are surface velocities of contacting surfaces, in this case the cylinder liner and the piston ring, respectively. Values for $f(k)$ from the compatibility condition in the case of the piston ring conjunctional gap are $k = 0$ and $f(k) = 4$.[29] By calculating the parameters using equations (9) and (10), the locations of the inlet stagnation and the outlet separation points from the centre of the ring can be found by obtaining the minimum film thickness and distribution across the conjunction. The work of Mohammadpour et al.[28] and that of Birkhoff and Hays[51] agree with this assumption.

Ring pack modelling: Starvation due to oil availability

Starvation occurs due to a physical lack of lubricant at any conjunctional inlet. The cylinder liner can be subdivided into three distinct regions according to the sources of lubricant supply (Figure 4). These are as follows:

- Region 1: between the oil control ring positions at the TDC and the bottom dead centre.
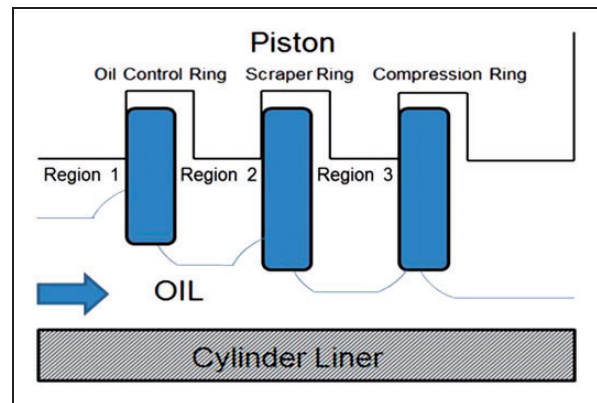

Figure 4. Schematic showing the flow of oil between the rings and liner for a downstroke.

- Region 2: between the scraper ring and the oil control ring positions at the TDC.
- Region 3: between the compression ring and the scraper ring positions at the TDC.

The available oil for a trailing ring is specified by the thickness of a lubricant layer, h_∞, on the free liner surface (Figure 1), left behind by a leading ring ahead of a trailing one[14]

$$h_\infty = \frac{\bar{q}_x - \bar{h}_T(x_e)\frac{dx_e}{dt}}{U - \frac{dx_e}{dt}} \tag{27}$$

$\bar{h}_T(x_e)\frac{dx_e}{dt}$ is the quantity of the accumulated oil at the exit. Tian et al.[14] provided an iterative method in order to obtain this value. In the current study, since the instantaneous value of x_e is determined from the Tipei's method, the variation in the location of the exit boundary condition can specify the amount of accumulated oil. If the ring is starved, a region of transition occurs where the lubricant attaches to the inlet location of the ring at x_i. This can be seen in Figure 1. $\bar{q}_x$ is the total oil flow as

$$\bar{q}_x = \frac{\rho h^3}{12\eta}\left[\frac{\partial p}{\partial x}\right] + (U)\left[\frac{\rho h}{2}\right] \tag{28}$$

Solution procedure

The following solution procedure is undertaken

1. At any crank angle position, determine which ring is the leading ring and which is the trailing one. For upstroke crank angles the top compression ring is the leading ring, whilst for downstroke motion the scraper ring is the leading ring.
2. Apply Tipei's conditions to find the inlet and exit locations for the leading ring. Solve Reynolds, film thickness and rheological state equations to calculate the minimum film thickness and friction due to the leading ring.
3. The inlet position depends on the film thickness affected by the position of the stagnation point (i.e. the inlet boundary). There is an intermediate iterative loop to converge for the inlet position and lubricant film thickness.
4. Using the results for the leading ring, the lubricant flow rate and thickness of film left on the free liner surface are determined.
5. Apply Tipei conditions to determine the inlet and exit locations for any trailing ring.
6. The same intermediate loop, as in step 3, is used for step 5.
7. Use step 2 for any trailing ring.

These steps of calculation are carried out at every crank angle position. A simplified version is shown in Figure 5.
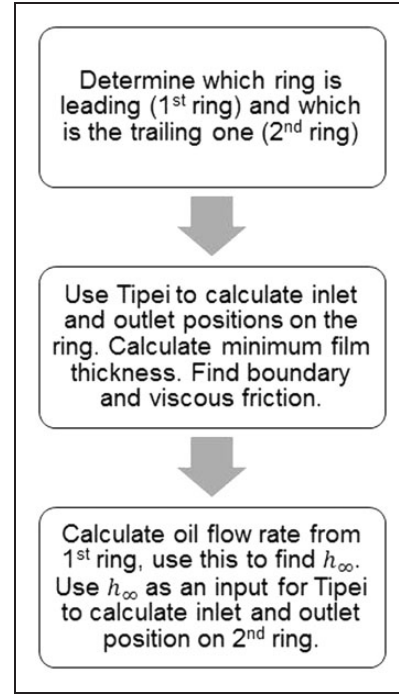

Figure 5. Condensed flow chart showing the solution procedure.

Table 1. Engine data.

Parameters	Values	Units
Torque	52.03	N m
No. of cylinders	4	–
Engine type	Gasoline SI	–
Crank pin radius, r	39.75	mm
Connecting rod length, l	138.1	mm
Bore nominal radius, r_0	44.52	mm
Ring crown height, c	10	µm
Ring axial face width, b	1.15	mm
Ring radial width, d	3.5	mm
Ring free end gap, g	10.5	mm

Table 2. Lubricant properties in atmospheric pressure and 40 °C.

Parameters	Values	Units
Lubricant viscosity, η_0	0.05	kg/ms
Lubricant density, ρ_0	833	kg/m^3
α_0	1×10^{-8}	m^2/N
Lubricant Eyring shear stress, τ_0	2	MPa

Results and discussion

A four-cylinder, four-stroke gasoline engine of a C-segment vehicle is studied here. The engine data are listed in Table 1. The lubricant rheological data, as well as surface parameters and material properties are listed in Tables 2 and 3. The engine speed used for the

current simulation study is 1500 r/min, corresponding to 35 km/h on the New European Drive Cycle with vehicle driven in third gear, with an output torque of 52.03 N m.

The variation in the minimum lubricant film thickness and total cyclic friction is predicted for both the

Table 3. Material properties and surface topographical parameters.

Parameters	Values	Units
Liner material	Grey cast iron	–
Modulus elasticity of the liner material	92.3	GPa
Poisson's ratio for the liner material	0.211	–
Density for the liner material	7200	kg/m^3
Ring material	Steel SAE 9254	–
Modulus elasticity of the ring material	203	GPa
Poisson's ratio for the ring material	0.3	–
Roughness parameter ($\zeta K \sigma$)	0.04	–
Measure of asperity gradient (σ/K)	0.001	–
Shear strength of asperities (ς)	0.17	–
Density for ring material	7700	kg/m^3

top compression ring and a scraper ring of the same conjunctional dimensions. The crank angle $\theta = 0°$ marks the position of TDC at the onset of power stroke. The maximum combustion pressure occurs at the crank angle $\theta = 20°$ in the case of this engine. Figure 6 shows the combustion pressure curve, P_c, for a complete engine cycle. It has been assumed that the inter-ring pressure is half that of the combustion pressure in this analysis. Figure 7 shows the variation in the measured liner surface temperature. The measured liner temperature is used to adjust the lubricant viscosity and density in the analysis. It is shown, both through measurement and in-depth analysis, that the liner temperature governs the lubricant temperature in passage through the ring pack.[52,53] Morris et al.[15] showed that any rise in lubricant temperature as the result of viscous shear in transition through ring–liner contact is small compared with its rise due to convection from the surface of the liner.

Application of zero reverse inlet boundary flow to the top compression ring

In order to understand the effect of starvation due to inlet counter flow prior to the stagnation boundary, the in-bound flow into the top compression ring–liner
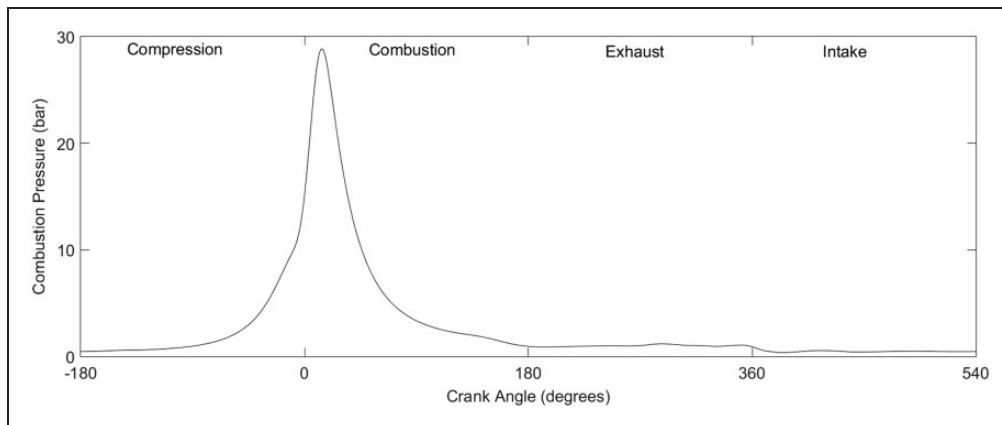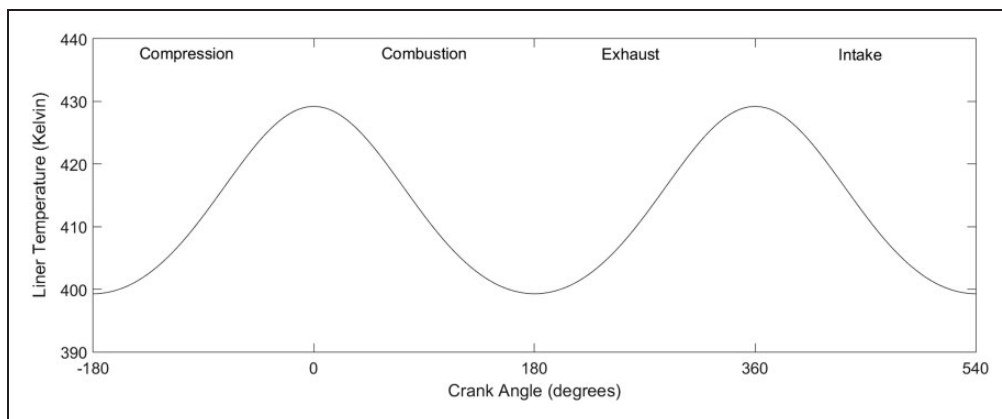

Figure 6. Combustion pressure.

Figure 7. Measured liner temperature.

conjunction is analysed. Figures 8 and 9 demonstrate that there is a reduction in the film thickness and an increase in total cyclic friction when the zero reverse boundary condition is used. The most significant effect on generated friction occurs at the piston reversal at the TDC, in transition from compression to power stroke. There is an increase of 50% in friction. This is mainly due to an increase in asperity interactions. The straight line in Figure 8 shows the onset of asperity interaction (i.e. $\lambda = 1$). It is clear that by taking into account the effect of starvation, there is a greater contribution due to boundary friction.

The ring pack model

It is possible to calculate the minimum lubricant film thickness and generated friction for a series of piston rings based upon lubricant availability on the free liner surface. Figure 10 shows the minimum film thickness for the top compression ring and the scraper ring, and the quantity of lubricant film available on

the free liner surface h_∞. In the upstroke, the top compression ring acts as the leading ring. It is assumed that it enjoys a sufficient supply of lubricant at its inlet meniscus. The only source of conjunctional starvation under this condition is that due to the counter flow prior to the stagnation point. The inlet of the scraper ring, trailing behind the compression ring, is fed by the layer of the lubricant on the free surface of the liner, h_∞, left post the passage of the compression ring. The method expounded by Tipei[30] and highlighted above is used to predict the potential reverse flow. This shows that the film thickness for the scraper ring is 70–74% lower than the top compression ring. In the downstroke, the roles of the leading and trailing rings are reversed in the analysis. Consequently, the film thickness for the top compression ring is significantly reduced, indicating starvation due to a lack of lubricant availability as well as due to counter flow at its inlet. Figure 11 shows the generated friction for each ring along with the total friction predicted for the complete ring pack used in the analysis. The variation in friction (Figure 11) corresponds
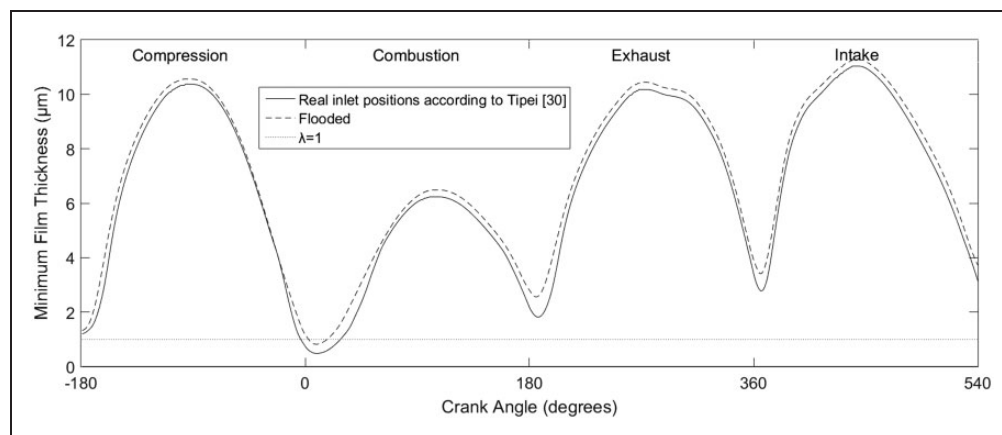

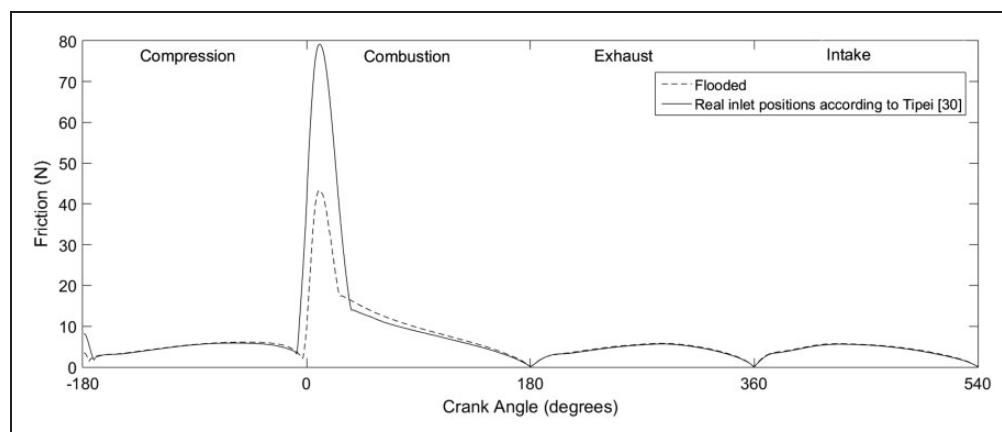**Figure 8.** Cyclic variation of minimum film thickness.

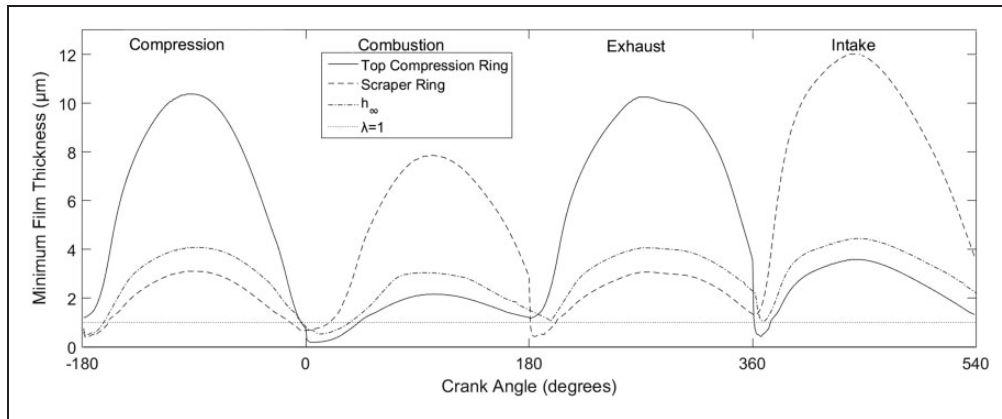**Figure 9.** Cyclic total (combined viscous and boundary) friction.

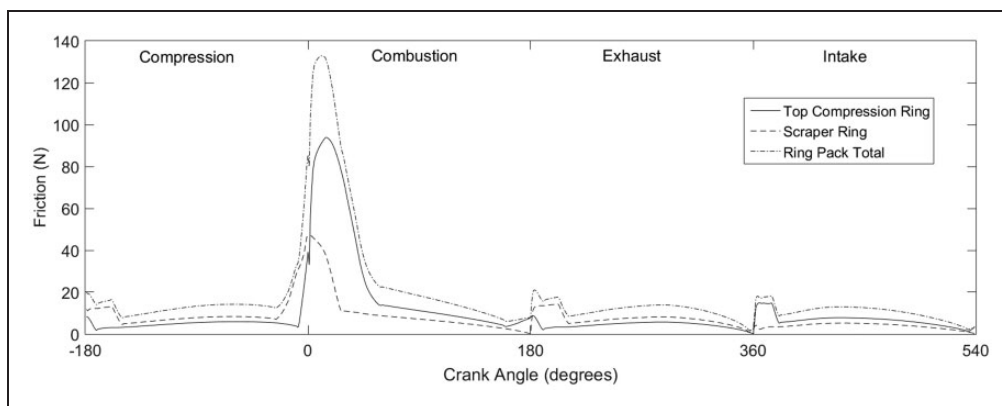**Figure 10.** Minimum oil film thickness.

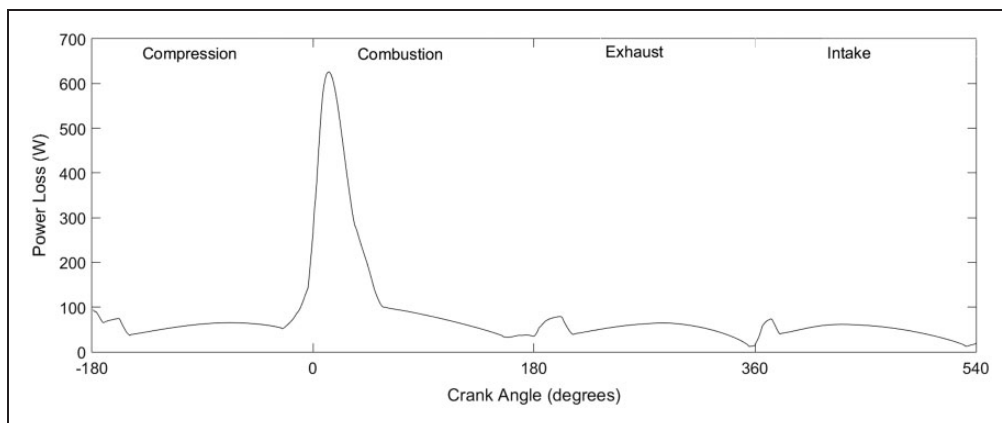**Figure 11.** Cyclic friction.

Figure 12. Total power loss for the ring pack.

directly to the predicted film thickness (Figure 10). Due to the omission of an oil control ring in the current analysis, there may be a thicker predicted film.

Figure 12 shows the total predicted power loss due to friction in the ring pack. It can be seen that viscous friction plays a dominant role in the compression, exhaust and intake strokes. Thus, an effective way of reducing friction in this conjunction would be to reduce the lubricant viscosity.[54] However, in the

combustion stroke there is also a considerable contribution from boundary friction, thus power loss due to a thinner lubricant film and higher asperity interaction inside the contact. This finding conforms to previously reported experiments, where boundary interactions were found to be dominant in the combustion stroke.[27]

Figures 13 and 14 show the realistic inlet and outlet positions (as opposed to the generally assumed
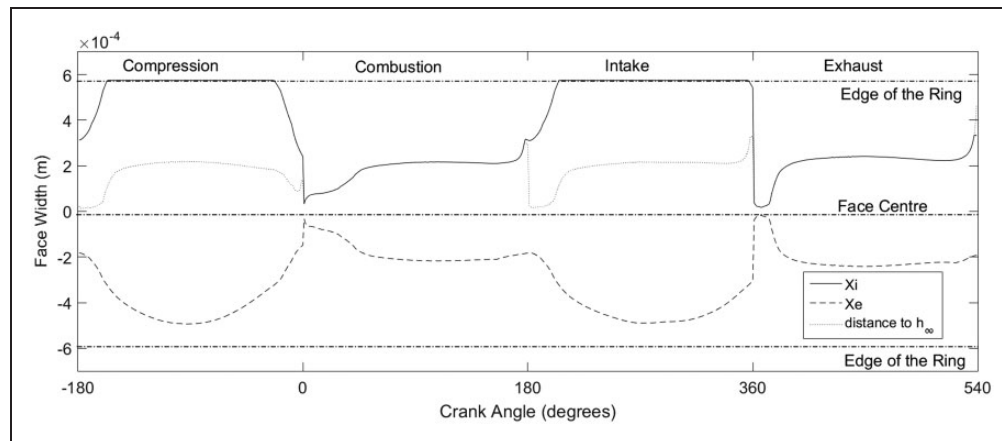
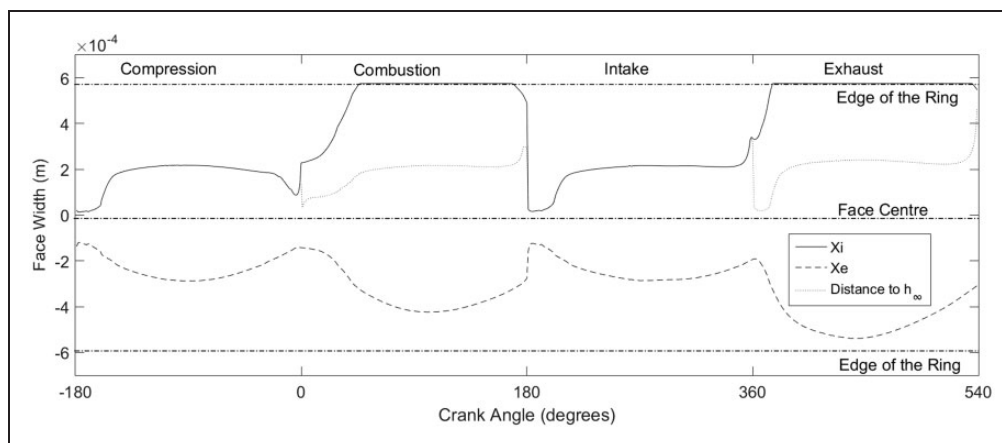**Figure 13.** Inlet and outlet locations of the top compression ring.

Figure 14. Inlet and outlet locations of the scraper ring.

idealised ones) calculated for the top compression ring and the scraper ring, respectively. The dot-dashed lines in each figure represent the top and bottom land of the ring. It should be noted that for the fully flooded case the top or bottom land would be used as the inlet. However, this analysis shows that for both rings in both upstroke and downstroke motions there would be regions with insufficient lubricant availability to warrant an assumed fully flooded inlet.

Concluding remarks

The paper presents a two-dimensional model of a piston ring pack comprising of a compression ring and scraper ring capable of predicting the minimum film thickness, friction and total power loss, taking into account two types of starvation. The analysis shows that by calculating the correct inlet and outlet boundary positions the available oil can be determined for system-level analysis of a ring pack, thus tackling both of the main sources of starvation. The first source is due to a physical lack of lubricant (i.e. a starved meniscus), whilst the second source is because of reverse (counter) flow at the conjunctional inlet.

Such an approach has not hitherto been reported in literature for the analysis of a piston ring pack. By correct positioning of the inlet boundary at the flow stagnation point, it is shown that there is a reduction in the thickness of the entrained lubricant into the conjunction and thus an increased overall friction.

ORCID iD

M Mohammadpour http://orcid.org/0000-0002-5312-3229

References

1. King J. *The King review of low-carbon cars: Part I: the potential for CO_2 reduction*. London: Office of Public Sector Information, HM Treasury, HMSO, 2007.
2. Tung SC and McMillan ML. Automotive tribology overview of current advances and challenges for the future. *Tribol Int* 2004; 37: 517–536.
3. Fitzsimons B. Introduction to the importance of fuel efficiency and role of the Encyclopaedic research project. In: *IMechE seminar: a drive for fuel efficiency*, Loughborough, UK, 2011.
4. Holmberg K, Andersson P and Erdemir A. Global energy consumption due to friction in passenger cars. *Tribol Int* 2012; 47: 221–234.
5. Wong VW and Hoult DP. Experimental survey of lubricant-film characteristics and oil consumption in a small diesel engine. SAE technical paper 932789, 1989.
6. Burnett PJ. Relationship between oil consumption, deposit formation and piston ring motion for single-cylinder diesel engines. SAE technical paper 920089, 1992.
7. Dowson D, Economou PN, Ruddy BL, et al. Piston ring lubrication – part II. Theoretical analysis of a single ring and a complete ring pack. In: *Energy conservation through the field of film lubrication technology: frontiers in research and design, winter annual meeting of ASME*. New York: ASME, 1979, pp.23–52.
8. Hu Y, Cheng HS, Arai T, et al. Numerical simulation of piston ring in mixed lubrication – a nonaxisymmetrical analysis. *Trans ASME J Tribol* 1994; 116: 470–478.
9. Jeng YR. Friction and lubrication analysis of a piston-ring pack. SAE paper 920492, 1992.
10. Jeng YR. Theoretical analysis of piston-ring lubrication Part I – fully flooded lubrication. *Tribol Trans* 1992; 35: 696–706.
11. Jeng YR. Theoretical analysis of piston-ring lubrication Part II-starved lubrication and its application to a complete ring pack. *Tribol Trans* 1992; 35: 707–714.
12. Taylor RI, Brown MA, Thompson DM, et al. The influence of lubricant rheology on friction in the piston ring-pack. SAE paper 941981, 1994.
13. Kerribar R, Dursunkaya Z and Flemming MF. An integrated model of ring pack performance. *Trans ASME J Eng Gas Turbines Power* 1991; 113: 382–389.
14. Tian T, Wong VW and Heywood JB. A piston ring-pack film thickness and friction model for multigrade oils and rough surfaces. SAE technical paper 962032, 1996.
15. Morris N, Rahmani R, Rahnejat H, et al. Tribology of piston compression ring conjunction under transient thermal mixed regime of lubrication. *Tribol Int* 2012; 59: 248–258.
16. Rahmani R, Theodossiades S, Rahnejat H, et al. Transient elastohydrodynamic lubrication of rough new or worn piston conjunction with an out-of-round cylinder bore. *Proc IMechE, Part J: J Engineering Tribology* 2012; 226: 284–305.
17. Ma MT, Sherrington I and Smith EH. Implementation of an algorithm to model the starved lubrication of a piston ring in distorted bores: predicton of oil flow and onset of gas blow-by. *Proc IMechE, Part J: J Engineering Tribology* 1996; 210: 29–44.
18. Ma MT, Sherrington I and Smith EH. Analysis of lubrication and friction for a complete piston-ring pack with an improved oil availability model. Part 1: circumferentially uniform film. *Proc IMechE, Part J: J Engineering Tribology* 1997; 211: 1–15.
19. Ma MT, Sherrington I and Smith EH. Analysis of lubrication and friction for a complete piston-ring pack with an improved oil availability model. Part 2: circumferentially variable film. *Proc IMechE, Part J: J Engineering Tribology* 1997; 211: 17–27.
20. Bewsher SR, Turnbull R, Mohammadpour M, et al. Effect of cylinder de-activation on the tribological performance of compression ring conjunction. *Proc IMechE, Part J: J Engineering Tribology* 2016; 231: 997–1006.
21. AVL, EXCITE^{TM} Piston&Rings Theory, Version 2017.
22. Hamatake T, Kitahara T, Wakuri Y, et al. Friction characteristics of piston rings in a reciprocating engine. *Lubricat Sci* 1993; 6: 21–40.
23. Patir N and Cheng HS. An average flow model for determining the effects of three dimensional roughness on partial hydrodynamic lubrication. *Trans ASME J Lubricat Technol* 1978; 100: 12.
24. Patir N and Cheng HS. Application of average flow model to lubrication between rough sliding surfaces. *Trans ASME J Lubricat Technol* 1979; 101: 220–230.
25. Sherrington I. Measurement techniques for piston-ring tribology. In: H Rahnejat (ed.) *Tribology and dynamics of engine and powertrain – fundamentals, applications & future trends*. Oxford, UK: Woodhead Publishing, 2010, p.387.
26. Furuhama S and Sasaki S. New device for the measurement of piston frictional forces in small engines. SAE technical paper 831284, 1983.
27. Gore M, Theaker M, Howell-Smith S, et al. Direct measurement of piston friction of internal-combustion engines using the floating-liner principle. *Proc IMechE, Part D: J Automobile Engineering* 2014; 228: 334–354.
28. Mohammadpour M, Johns-Rahnejat PM, Rahnejat H, et al. Boundary conditions for elastohydrodynamics of circular point contacts. *Tribol Lett* 2014; 53: 107–118.
29. Shahmohamadi H, Mohammadpour M, Rahmani R, et al. On the boundary condition in multi-phase flow through the piston ring-cylinder liner conjunction. *Tribol Int* 2015; 90: 164–174.
30. Tipei N. Boundary conditions of viscous flow between surfaces with rolling and sliding motion. *Trans ASME, J of Lubrication Tech* 1968; 90: 254–261.
31. Tipei N. *Theory of lubrication*. Stanford, CA: Stanford University Press, 1962.
32. Gore M, Rahmani R, Rahnejat H, et al. Assessment of friction from compression ring conjunction of a high-performance internal combustion engine: a combined numerical and experimental study. *Proc IMechE, Part C: J Mechanical Engineering Science* 2016; 230: 2073–2085.
33. Dowson D and Higginson GR. *Elasto-hydrodynamic lubrication*. 2nd SI edition. Oxford: Pergamon Press, 1977.
34. Gohar R and Rahnejat H. *Fundamentals of tribology*. London: Imperial College Press, 2008.
35. Barus C. Isothermals isopietics and isometrics in relationship to viscosity. *Am J Sci 3rd Ser* 1893; 45: 87–96.
36. Roelands CJ. *Correlation aspects of the viscosity-temperature-pressure relationships of lubricating oils*. PhD thesis, Delft University of Technology, the Netherlands, 1966.

37. Houpert L. New results of traction force calculations in elastohydrodynamic contacts. *Trans ASME, J Tribol* 1985; 107: 241–248.

38. Bolander NW, Steenwyk BD, Sadeghi F, et al. Lubrication regime transitions at the piston ring-cylinder liner interface. *Proc IMechE, Part J: J Engineering Tribology* 2005; 219: 19–31.

39. Mishra PC, Balakrishnan S and Rahnejat H. Tribology of compression ring-to-cylinder contact at reversal. *Proc IMechE, Part J: J Engineering Tribology* 2008; 222: 815–826.

40. Baker C, Theodossiades S, Rahmani R, et al. On the transient three-dimensional tribodynamics of internal combustion engine top compression ring. *J Eng Gas Turbines Power* 2017; 139: 062801.

41. Rycroft JE, Taylor RI and Scales LE. Elastohydrodynamic effects in piston ring lubrication in modern gasoline and diesel engines. *Tribol Interf Eng Ser* 1997; 32: 49–54.

42. Greenwood JA and Tripp JH. The elastic contact of rough spheres. *J Appl Mech* 1967; 34: 153–159.

43. Greenwood JA and Tripp JH. The contact of two nominally flat rough surfaces. *Proc Instn Mech Engrs* 1970–1971; 185: 625–634.

44. Akalin O and Newaz GM. Piston ring-cylinder bore friction modelling in mixed lubrication regime: Part I – analytical results. *Trans ASME J Tribol* 1999; 123: 211–218.

45. Shahmohamadi H, Rahmani R, Rahnejat H, et al. Thermo-mixed hydrodynamics of piston compression ring conjunction. *Tribol Lett* 2013; 51: 323–340.

46. Vladescu S-C, Olver AV, Pegg IG, et al. Combines friction and wear reduction in a reciprocating contact through laser surface texturing. *Wear* 2016; 358–359: 51–61.

47. Vladescu S-C, Ciniero A, Tufail K, et al. Looking into a laser textured piston ring-liner contact. *Tribol Int* 2017; 115: 140–153.

48. Swift HW. The stability of lubricating films in journal bearings. *Proc Inst Civil Eng* 1932; 233: 267–288.

49. Steiber W. *Das-Schwimmlager: hydrodynamische Theorie des Gleitlagers*. Berlin: V.D.I., 1933, p.106.

50. Arcoumanis C, Duszynski M, Flora H, et al. Development of a piston-ring lubrication test-rig and investigation of boundary conditions for modelling lubricant film properties. SAE technical paper 952468, 1995.

51. Birkhoff G and Hays DF. Free boundaries in partial lubrication. *J Math Phys* 1963; 42: 126–138.

52. Ma Z, Henein NA and Bryzik W. A model for wear and friction in cylinder liners and piston rings. *Tribol Trans* 2006; 49: 315–327.

53. Rahmani R, Rahnejat H, Fitzsimons B, et al. The effect of cylinder liner operating temperature on frictional loss and engine emissions in piston ring conjunction. *Appl Energy* 2017; 191: 568–581.

54. Taylor RI and Coy RC. Improved fuel efficiency by lubricant design: a review. *Proc IMechE, Part J: J Engineering Tribology* 2000; 214: 1–15.

Appendix

Notation

A	apparent contact area
A_a	asperity contact area
b	ring face width
c	ring crown height
d	ring radial width (thickness)
f	total generated contact friction
f_b	boundary friction
f_v	viscous friction
F	applied contact load
F_2	statistical function
$F_{5/2}$	statistical function
F_e	ring elastic force (ring tension)
F_g	gas force acting behind the ring inner rim
g	ring end gap
h	lubricant film thickness
h_m	minimum lubricant film thickness
h_s	axial profile of the ring
h_∞	thickness on lubricant layer on free liner surface
I	second area moment of inertia
k	ratio of contiguous surface velocities
K	conformability coefficient (factor)
l	ring circumferential length (bore perimeter)
ℓ	connecting rod length
n	iteration counter
p	gauge pressure
p_e	elastic pressure
P_a	pressure at the ring inlet conjunction
P_c	combustion pressure
P_{cav}	cavitation pressure
q	volumetric flow rate
r	crank pin radius
r_0	nominal bore radius
S_0	temperature viscosity index
t	time
$\underline{U}$	sliding velocity
V	velocity vector
W	total contact reaction
W_a	load share of asperities
W_h	hydrodynamic reaction
x	direction along the ring face width
x_c	lubricant film rupture point
x_1	ring inlet position
x_2	ring outlet position
y	direction along the bore circumference
Z	pressure viscosity index

Greek symbols

α	pressure–viscosity coefficient
α^*	modified pressure–viscosity coefficient
β	temperature–viscosity coefficient
ζ	number of asperities per unit area of contact
η	lubricant dynamic viscosity
η_0	atmospheric dynamic viscosity
θ	liner temperature
θ_0	reference temperature

θ_i	ratio of the film thickness at the stagnation point to that at contact centre	σ	root mean square (RMS) composite surface roughness
θ_e	ratio of the film thickness at the rupture point to that at contact centre	ς	pressure coefficient of boundary shear strength of asperities
κ	average asperity tip radius of curvature	τ_0	Eyring shear stress
λ	Stribeck's oil film parameter	φ	crank angle
ρ	lubricant density	ω	engine speed
ρ_0	lubricant density at atmospheric pressure		